Nuclear Engineering and Technology 53 (2021) 2640–2645

Contents lists available at ScienceDirect

Nuclear Engineering and Technology

journal homepage: www.elsevier.com/locate/net

Original Article

Development and performance evaluation of large-area hybrid gamma imager (LAHGI)

Hyun Su Lee [a], Jae Hyeon Kim [a, b], Junyoung Lee [a], Chan Hyeong Kim [a, *]

[a] Department of Nuclear Engineering, Hanyang University, Seoul, 04763, Republic of Korea
[b] Radiation Research Division, Korea Atomic Energy Research Institute, Jeongeup, 56212, Republic of Korea

ARTICLE INFO

Article history:
Received 2 October 2020
Received in revised form
23 December 2020
Accepted 30 January 2021
Available online 3 February 2021

Keywords:
Hybrid imaging
Compton imaging
Coded aperture imaging
Scintillation detector

ABSTRACT

We report the development of a gamma-ray imaging device, named Large-Area Hybrid Gamma Imager (LAHGI), featuring high imaging sensitivity and good imaging resolution over a broad energy range. A hybrid collimation method, which combines mechanical and electronic collimation, is employed for a stable imaging performance based on large-area scintillation detectors for high imaging sensitivity. The system comprises two monolithic position-sensitive NaI(Tl) scintillation detectors with a crystal area of 27 × 27 cm^2 and a tungsten coded aperture mask with a modified uniformly redundant array (MURA) pattern. The performance of the system was evaluated under several source conditions. The system showed good imaging resolution (i.e., 6.0–8.9° FWHM) for the entire energy range of 59.5–1330 keV considered in the present study. It also showed very high imaging sensitivity, successfully imaging a 253 μCi ^{137}Cs source located 15 m away in 1 min; this performance is notable considering that the dose rate at the front surface of the system, due to the existence of the ^{137}Cs source, was only 0.003 μSv/h, which corresponds to ~3% of the background level.

1. Introduction

Gamma-ray imaging, providing position information of radiation sources, has taken on an important role in the nuclear industry. Especially for applications such as environmental remediation and homeland security, gamma imaging devices with high sensitivity and reasonable imaging resolution over a broad energy range are required [1].

Recently, a high-sensitivity Compton imaging system, called the Large-Area Compton Camera (LACC) [2], was developed to meet the demand for high imaging sensitivity and good imaging resolution. By employing large-area monolithic scintillation detectors, the LACC delivered higher imaging sensitivity than could other Compton cameras that focused mostly on hand-held portability [3–9], and it also featured 3-D imaging capability for near-fields [2]. However, the LACC was of practical utility only for energies higher than a few hundred keV, due to the principal limitations of its electronic collimation based on Compton kinematics, which is incurred by large energy measurement uncertainty and a low probability of effective event occurrence at lower energies.

One of the approaches to solve the problem of the energy dependency of gamma imaging is using both mechanical and electronic collimation [10,11]. The hybrid imaging, which combines the data from two different imaging methods implemented in a single system, was proposed by Lee [12], and its advantage over conventional imaging methods was demonstrated in several studies [13–17]. However, the imaging sensitivity was still limited in hand-held hybrid imaging systems [14,15], and the high sensitivity system [16] requires a vehicle to move, which discourages flexible application on indoor and outdoor.

In the present study, a gamma imaging device with high imaging sensitivity and reasonable imaging resolution (<10°) over a broad energy range (50 keV – a few MeV), named Large-Area Hybrid Gamma Imager (LAHGI), was developed for use in environmental remediation and homeland security using two large-area monolithic position-sensitive NaI(Tl) scintillation detectors and a tungsten collimator mask. The LAHGI achieved high imaging sensitivity based on the large-area detectors at the cost of size and weight, but mounted on a trolly, the system is still mobile and applicable both indoors and outdoors. The LAHGI was tested for several source conditions, and its performance was evaluated.

* Corresponding author.
E-mail address: chkim@hanyang.ac.kr (C.H. Kim).

https://doi.org/10.1016/j.net.2021.01.036

2. Materials and methods

The LAHGI developed in the present study consists of a modified uniformly redundant array (MURA) coded aperture mask [18] and two large-area monolithic position-sensitive scintillator detectors [19], as shown in Fig. 1. The detectors' design was derived from the LACC [2]. Each of the detectors is composed of a monolithic NaI(Tl) scintillator crystal (27 × 27 cm^2; Scintitech, Shirley, MA, USA), optically coupled with a 6 × 6 compact array of square photomultiplier tubes (PMTs; XP3290; Photonis, Mérignac, France). The gamma interactions are read out by a multiplexer-based in-house readout system, as shown in Fig. 2. The signals from the 36 PMTs for each detector are processed by shaping amplifiers, sample-and-holders, and a multiplexer, and are then digitized by a 14-bit analog-to-digital converter (ADC) on a field programmable gate array (FPGA)-based data acquisition system. Single events in the front detector for coded aperture imaging, and coincidence events in both detectors for Compton imaging, are recorded according to the dedicated trigger logics. The event energies and locations are estimated from 36 PMT signals, with an energy resolution of 7.9% full width at half maximum (FWHM) for a 662 keV gamma ray of ^{137}Cs and a spatial resolution of ~5 mm with the maximum likelihood position estimation (MLPE) technique [20], which estimates interaction position by comparing detector signals to pre-measured calibration data. The thickness of the scintillator crystal of the front and back detector is 2 and 3 cm, respectively, as optimized for maximum sensitivity of Compton imaging. The front faces of the two detectors are separated by 25 cm.

The coded aperture mask is made of tungsten blocks (0.73 × 0.73 × 0.6 cm^3) assembled on a polymethyl methacrylate frame, following a 2 × 2 mosaic of rank 19 MURA pattern. The optimal thickness of the tungsten mask was derived to provide enough opaqueness at a few hundred keV gamma rays in consideration of a trade-off between the image contrast of coded aperture imaging and the sensitivity of Compton imaging. The assembled mask is fixed parallel to the front surface of the detector with screws and spacers. The mask-to-detector distance is set to 6 cm, as designed for coded aperture imaging to provide a field of view (FOV) of ~130°, equal to that of Compton imaging. Additional details on the design of the LAHGI can be found elsewhere [21]. The LAHGI, including the detectors, the mask, and the signal processing system, is mounted on a trolley for mobility. The LAHGI weighs about 82 kg, excluding the laptop computer and the trolley.

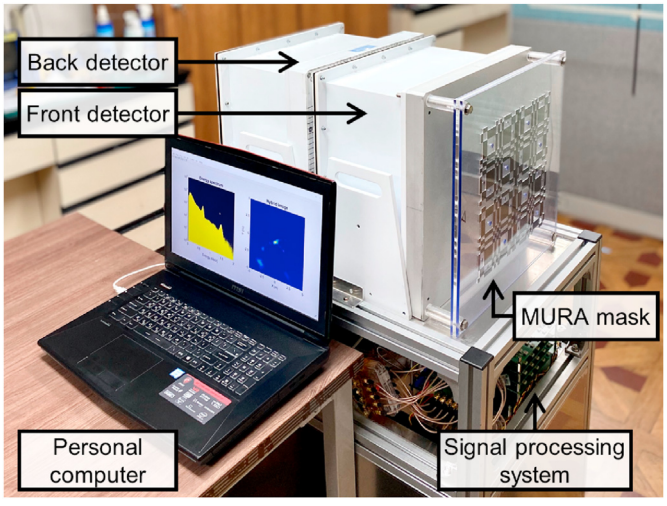

Fig. 1. Developed LAHGI mounted on trolley. The mask is fixed to the front detector.

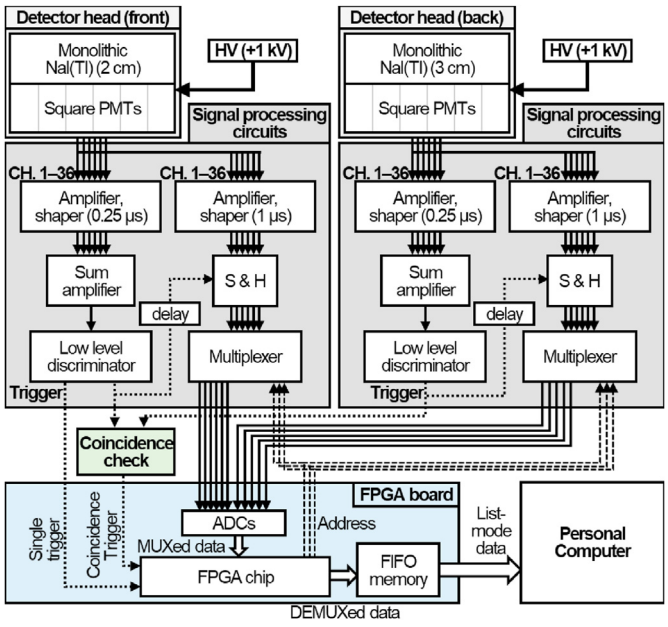

Fig. 2. Schematic of signal flow of developed LAHGI.

Effective events were selected from the measured data according to energy: full energy events on the front detector for coded aperture imaging, and coincidence events that sum of measured energies from two detectors corresponds to the source energy for Compton imaging. A set of list-mode data composed of the coordinates of interaction position and energy is processed with a maximum-likelihood estimation-maximization (ML-EM) image reconstruction algorithm [22] for hybrid imaging [13], given by

$$\lambda_j^{n+1} = \lambda_j^n \frac{\sum_i \left(c_{ij}^M Y_i^M \Big/ \sum_k c_{ik}^M \lambda_k^n \right) + \sum_i \left(c_{ij}^C Y_i^C \Big/ \sum_k c_{ik}^C \lambda_k^n \right)}{S_j^M + S_j^C}$$

where the symbols are defined as: λ_j^n is the intensity of image pixel j on the nth iteration; Y_i is the number of events recorded at ith pixel of the detector; c_{ij} is the probability that a gamma ray leaving image pixel j is detected at detector pixel i (i.e. the system matrix); S_j is the detection probability of a photon from image pixel j (i.e. the sensitivity image); and superscript M and C corresponds to MURA coded aperture imaging and Compton imaging, respectively.

The method of sensitivity image calculation for Compton imaging is based on Muñoz et al.'s [23], in which the sensitivity image for a given gamma energy is computed by randomly sampling a source position from an image pixel and an interaction position from the volume of each detector and by integrating the probability of the sampled dataset (i.e., Monte Carlo integration). Similar approach is applied to calculating system matrix of the coded aperture, except that the interaction position is sampled from the pixel of the front detector and the probability is calculated pixel by pixel. The sensitivity image of coded aperture imaging is sum of its system matrix. The probability of each dataset is calculated considering a solid angle, attenuation from the mask and the crystal, and the interaction probability in the detector (i.e., photoelectric absorption for coded aperture imaging and Compton scattering and subsequent absorption for Compton imaging). The system matrix for Compton imaging data is calculated only for the measured event (i.e., list-mode ML-EM) to reduce computational load, otherwise, it would require tremendous resources to calculate the system matrix for all possible events.

In the present study, the hybrid imaging was applied to all gamma rays, i.e., regardless of their energies. While some literature [11] suggests using hybrid imaging within a certain energy range beneficial for hybrid collimation, the findings from our recent simulation study [21], in which hybrid imaging provided higher sensitivity (i.e. a lower value for minimum detectable activity) for a very wide energy range, encouraged us to use the hybrid imaging method for the entire energy range considered in the present study.

The image space was set as a 300 × 300 pixel square plane at a given source distance for each measurement condition. The size of the image space was 6 m × 6 m in all case except for different source distance conditions (chapter 3.3), of which the size of image space is specified separately. The iteration number in the ML-EM reconstruction was empirically selected as 30, considering the variation of imaging resolution as a function of iteration number. The data acquisition and image processing were conducted using a MATLAB-based in-house program running on a personal computer (Intel Core i7-6700 CPU at 3.40 GHz).

3. Results and discussion

The performance of the developed system (LAHGI) was evaluated under several source conditions entailing different energies, positions, and activities. The imaging time was 1 min in all cases considered in the present study. The imaging resolution was evaluated as an angle that corresponds to FWHM of the reconstructed image. The FWHM was measured in Cartesian coordinate and then converted into angle trigonometrically considering the source position.

3.1. Single point source with different energies

Four different isotopes were chosen to investigate the energy dependency of the system performance: ^{241}Am, ^{133}Ba, ^{137}Cs, and ^{60}Co, with activities of 11.0, 31.7, 18.7, and 7.7 μCi, respectively. Each source was placed 3 m from the front surface of the imaging system. Energy window for each isotope is 45–75 keV, 320–390 keV, 600–720 keV, and 1110–1400 keV for ^{241}Am, ^{133}Ba, ^{137}Cs, and ^{60}Co, respectively. For ^{133}Ba, only 356 keV was considered. For ^{60}Co, both 1170 and 1330 keV gamma rays were considered. As shown in Fig. 3(a–d), the developed system with hybrid imaging provided a clear image of the source for all of the sources, with a positional error of less than 3 pixels (= 9 cm). When Compton imaging was used alone, on the other hand, low-energy gamma-ray sources, specifically ^{241}Am and ^{133}Ba, were not imaged, due to the low probability of Compton scattering and large energy measurement uncertainty. The number of coincidence events recorded from 1-min imaging was 0 and 70 for ^{241}Am and ^{133}Ba, respectively, both of which are insufficient for Compton imaging (Fig. 3(e and f)). For the 59.5 keV gamma rays of ^{241}Am, a Compton camera based on low-Z semiconductor detectors needs to be used, but it is impractical for a high-sensitivity system. In hybrid imaging, mechanical collimation is employed for the imaging of low-energy gamma rays. The imaging resolution of the LAHGI in the present study was evaluated as 8.9, 6.0, 8.0, and 8.5° FWHM for ^{241}Am, ^{133}Ba, ^{137}Cs, and ^{60}Co, respectively. The imaging resolution, when coded aperture was used separately, was 8.9, 6.1, 9.8, and 13.3° FWHM for ^{241}Am, ^{133}Ba, ^{137}Cs, and ^{60}Co, respectively. The high imaging resolutions were observed in higher energies, due to the gamma rays penetrating the mask. When the Compton events were combined, however, the imaging resolution improved. The very sharp Compton images of ^{137}Cs and ^{60}Co were due to multiple iterations of ML-EM reconstruction on an insufficient number of overlapped Compton cones. Such low counting statistics were partly caused by the mask's blocking of up to 50% of the source gamma rays, but such an effect is overcome when the information from the mechanical collimation is combined. Detection efficiency was defined as the ratio of net count of effective event to the total number of gamma rays incident on the surface of the first detector, i.e. intrinsic efficiency. Net count was used in the present study because the number of events originated from background radiation is considerable when the source activity is very low as current condition, and it may result in overestimation of efficiency. The detection efficiency of coded aperture events was 1.19×10^{-1}, 8.79×10^{-2}, 8.96×10^{-2}, and 6.04×10^{-2} for ^{241}Am, ^{133}Ba, ^{137}Cs, and ^{60}Co, respectively. The detection efficiency of Compton events was 4.63×10^{-3}, 2.80×10^{-3}, and 3.60×10^{-3} for ^{133}Ba, ^{137}Cs, and ^{60}Co, respectively. The detection efficiency of the LAHGI was compared with that of compact hybrid gamma camera [15]. In the literature, detection efficiency of the compact hybrid gamma camera was available only for 356, 662, and 1275 keV. The detection efficiencies of 356 and 662 keV were compared correspondingly,

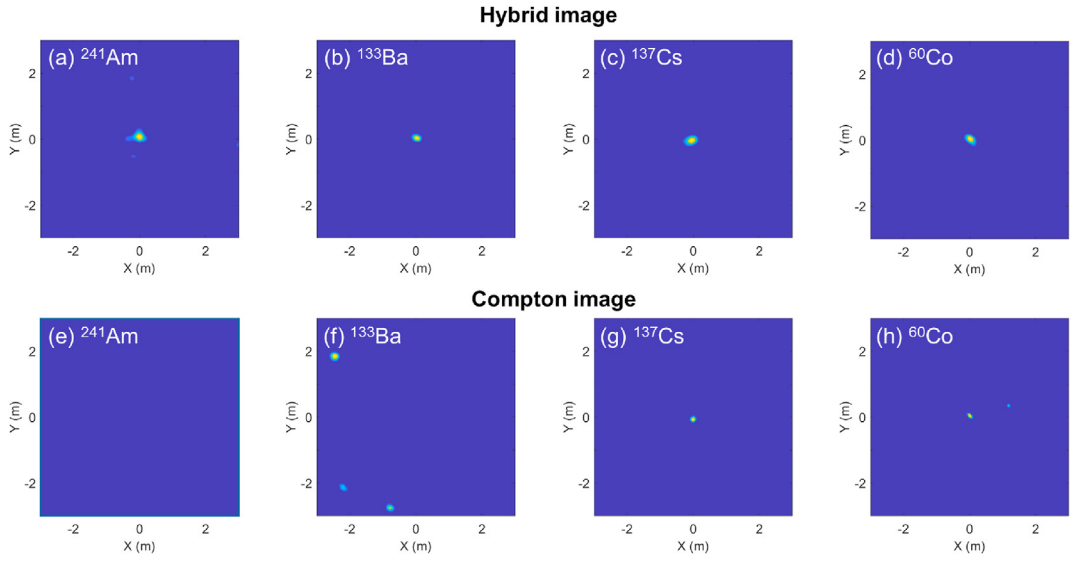

Fig. 3. Reconstructed images of different isotopes: (a, e) ^{241}Am, (b, f) ^{133}Ba, (c, g) ^{137}Cs, and (d, h) ^{60}Co; (a–d) hybrid image and (e–h) Compton image.

and detection efficiency of ^{60}Co was compared to that of 1275 keV. This approximation may be inaccurate; however, it could still offer a rough estimation. The detection efficiency of coded aperture imaging and Compton imaging of the LAHGI was 20–500 times and 20–110 times higher than that of previously developed system, respectively. Note that the compared detection efficiency is intrinsic efficiency, and when it comes to absolute efficiency, where solid angle taken by the detector is considered, the high efficiency of the LAHGI would be more prominent.

3.2. Single point source at off-axis position

A ^{137}Cs source was placed at off-axis positions with the off-axis angles of 20, 40, 60, and 80° (see Fig. 4) from the z-axis of the system, while maintaining the 3 m source-to-detector distance. The activity of the source was 18.7 μCi. The reconstructed images are shown in Fig. 4. The position of the source was clearly shown on the image for the 20, 40, and 60° positions (Fig. 4(a–c)). The actual source position was (1.03, 0, 2.82 m), (1.93, 0, 2.30 m), and (2.60, 0, 1.50 m) for 20, 40, and 60° positions, respectively, whereas the position of the pixel with the maximum intensity was (1.07, 0.05 m), (1.85, 0.02 m), and (2.68, 0.02 m) at corresponding z distance of the imaging space. The positional error in the xy direction was 5.8 cm, 8.2 cm, and 8.2 cm, respectively, which was less than 3 pixels of the image for the three cases, while some degradation of the imaging resolution was found at larger off-axis angles: 8.6° FWHM at the 20° position to 9.6° FWHM at the 60° position. Note that the imaging resolution was 8.0° at the 0° position (see Fig. 3(c)). One of the possible reasons for such an effect is that the image reconstruction was conducted on a Cartesian coordinate system, and that the back-projections of the events on the image plane were more oblique at greater off-axis positions. Also, the hole of the mask was partly blocked by the physical thickness of the mask at greater off-axis positions, which phenomenon is known as the vignette effect. For the source at the 80° position, outside of the FOV (±65°, theoretically estimated in a previous study) [21], the position of the source did not appear on the reconstructed image, as expected.

3.3. Single point source at different distances

The imaging sensitivity of the developed hybrid imager was evaluated by imaging a ^{137}Cs source at different distances. For this, the ^{137}Cs source with an activity of 253 μCi was located 5, 10, 15, and 20 m from the front surface of the LAHGI. The reconstructed images are shown in Fig. 5. On them, there was an apparent increase of noise with increasing source distance, resulting in a degradation of signal-to-noise ratio: from 22.9 for the source at 5 m, to 12.7 for the source at 15 m. Still, the positions were clearly visible for the 5, 10, and 15 m sources (Fig. 5(a–c)). For the source at 15 m, the dose rate from the source at the detector face was estimated to be 0.003 μSv/h, which corresponded to only ~3% of the background level (~0.1 μSv/h). When the source was placed at 20 m, making for a 0.0017 μSv/h dose rate at the detector, the source could not be distinguished in the image for 1-min imaging (Fig. 5(d)). By extending the measurement time to 5 min, however, we were able to image the source at the 20 m distance.

3.4. Two point sources with different separations

Imaging resolution is often evaluated as a point spread function (PSF), specifically by measuring the FWHM of an image for a point source. However, imaging resolution is sometimes overestimated as a result of excessive iteration in ML-EM; indeed, a sharper image from many iterations does not guarantee better imaging resolution, and sometimes results in more noise on the image. In the present study, imaging resolution evaluated for a single point source (see Fig. 3) was checked based on the following definition of *resolution*: the capability of resolving two closely positioned point sources. To that end, two ^{137}Cs sources with similar activities (i.e., 81.7 and 82.6 μCi) were placed on a plane 3 m from the detector face. The separation between the sources was 15.7, 31.4, 47.2, and 63 cm, equivalent to separation angles of 3, 6, 9, and 12°, respectively. The reconstructed hybrid image of each case and its profile is shown in Fig. 6. The two sources were not distinguished clearly on the image of 6° separation (Fig. 6(b)) but were almost distinguished on the image of 9° separation (Fig. 6(c)). These results agreed well with the

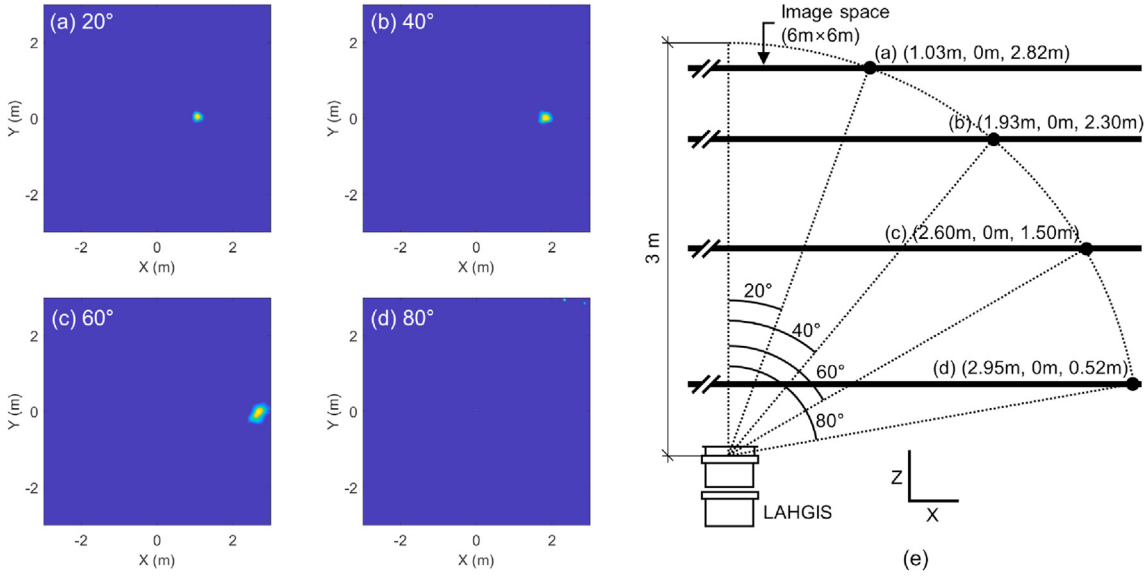

Fig. 4. Hybrid images of ^{137}Cs source at off-axis positions: (a) 20°, (b) 40°, (c) 60°, and (d) 80°. The experimental settings of the respective cases are shown in (e).

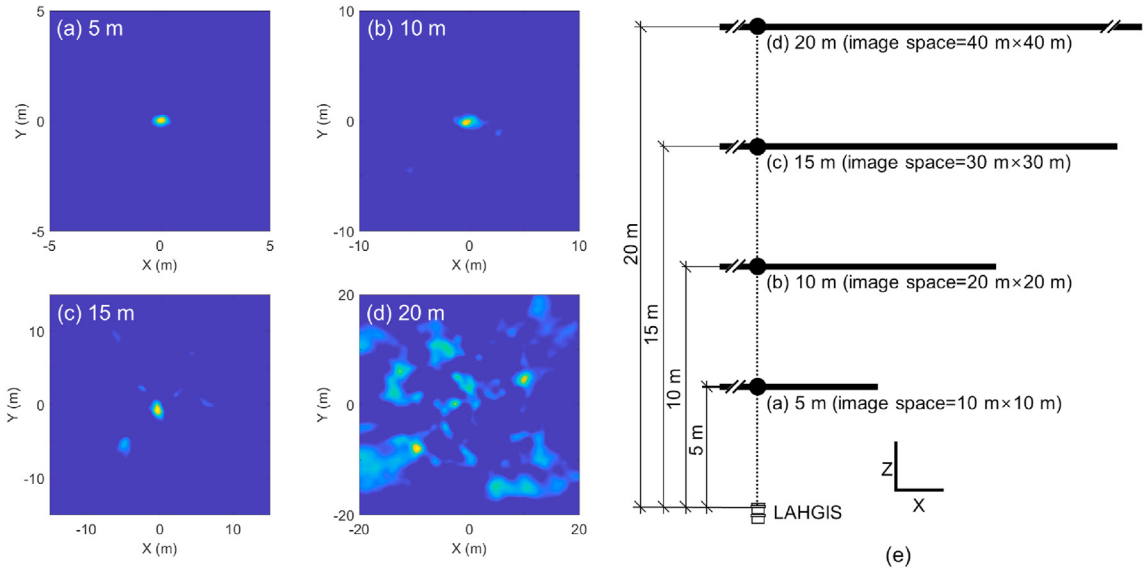

Fig. 5. Hybrid images of ^{137}Cs source at different distances: (a) 5 m, (b) 10 m, (c) 15 m, and (d) 20 m. The experimental settings of the respective cases are shown in (e).

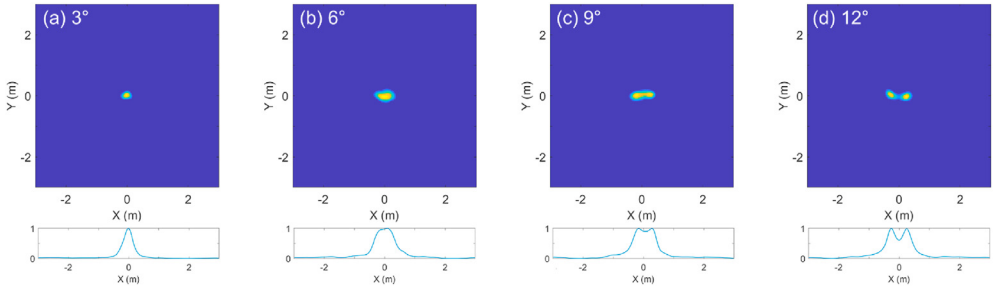

Fig. 6. Reconstructed images and profiles of two point sources with different separations: (a) 3°, (b) 6°, (c) 9°, and (d) 12°.

imaging resolution of 8.0° FWHM evaluated for the ^{137}Cs point source in Fig. 3.

3.5. Multiple point sources

Four point sources with different gamma-ray energies were placed on a plane 3 m from the image system, 50 cm off-axis (in the x or y direction from the center): ^{241}Am on the left (−0.5, 0, 3 m), ^{133}Ba on the top (0, 0.5, 3 m), ^{137}Cs on the bottom (0, −0.5, 3 m), and ^{60}Co on the right (0.5, 0, 3 m). The events from these sources were recorded simultaneously for 1 min, and then the images were reconstructed separately for each source by applying different energy windows according to the source energies. Fig. 7 shows the images of the four sources measured together but reconstructed separately. The four sources with energies ranging from 59.5 to 1330 keV were clearly imaged. In the image of ^{241}Am (Fig. 7(a)), some artifacts were found, mostly at the position of the ^{133}Ba source. Those seemingly had been caused by the ~30 keV X-rays and 81 keV gamma rays from the ^{133}Ba source, which came into the energy window for ^{241}Am (45–75 keV). Such artifacts can be reduced by narrowing the energy window or by introducing further analysis including nuclide information from gamma spectroscopy.

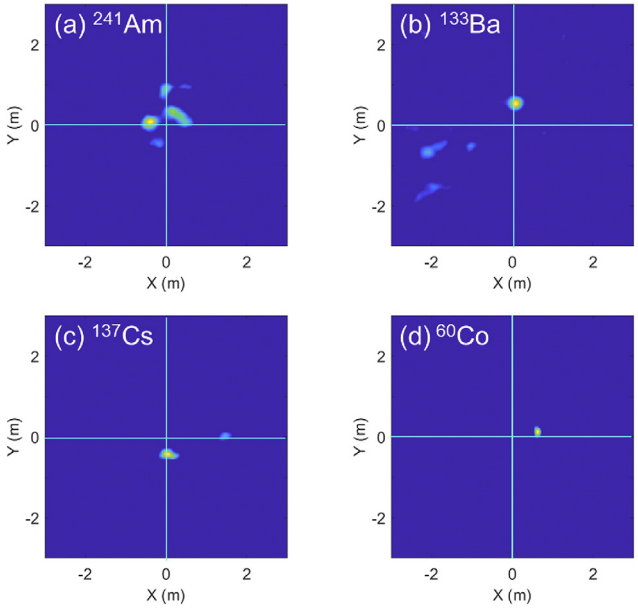

Fig. 7. Hybrid images of four sources measured at same time: (a) ^{241}Am, (b) ^{133}Ba, (c) ^{137}Cs, and (d) ^{60}Co.

4. Conclusion

In the present study, a high-sensitivity gamma imaging device utilizing a hybrid imaging method named LAHGI was developed by

adapting mechanical collimation to the LACC. The performance of the system was evaluated with several source conditions. The system showed good energy resolution (i.e., 6.0–8.9° FWHM) for the entire energy range of 59.5–1330 keV considered. The system also showed very high imaging sensitivity: it successfully imaged a 253 μCi ^{137}Cs source located 15 m from the imaging system with 1-min imaging, which is considered notable considering that the dose rate at the front surface of the imaging system due to the existence of the ^{137}Cs source was only 0.003 μSv/h, which corresponds to ~3% of background level. Future work will entail utilization of contextual sensors such as a range scanner and visual camera for improved imaging performance and provision of intuitive information.

Declaration of competing interest

The authors declare that they have no known competing financial interests or personal relationships that could have appeared to influence the work reported in this paper.

Acknowledgement

This work was partly supported by the National Research Foundation of Korea (NRF) grant funded by the Korea government(MSIT) [No. NRF-2017M2A8A4015258, NRF-2019M2D2A1A02059814], and Korea Institute of Energy Technology Evaluation and Planning(KETEP) grant funded by the Korea government(MOTIE) [No. 20191510301040].

References

[1] L.E. Smith, Z. He, D.K. Wehe, G.F. Knoll, S.J. Wilderman, Design and modeling of the hybrid portable gamma camera system, IEEE Trans. Nucl. Sci. 45 (1998) 963–969.
[2] Y. Kim, J.H. Kim, J. Lee, C.H. Kim, Large-area Compton camera for high-speed and 3-D imaging, IEEE Trans. Nucl. Sci. 65 (2018) 2817–2822.
[3] M. Galloway, A. Zoglauer, M. Amman, S.E. Boggs, P.N. Luke, Simulation and detector response for the high efficiency multimode imager, Nucl. Instrum. Methods A. 652 (2011) 641–645.
[4] A. Kishimoto, J. Kataoka, T. Nishiyama, T. Fujita, K. Takeuchi, H. Okochi, H. Ogata, H. Kuroshima, S. Ohsuka, S. Nakamura, M. Hirayanagi, S. Adachi, T. Uchiyama, H. Suzuki, Performance and field tests of a handheld Compton camera using 3-D position-sensitive scintillators coupled to multi-pixel photon counter arrays, J. Instrum. 9 (2014).
[5] S. Takeda, A. Harayama, Y. Ichinohe, H. Odaka, S. Watanabe, T. Takahashi, H. Tajima, K. Genba, D. Matsuura, H. Ikebuchi, Y. Kuroda, T. Tomonaka, A portable Si/CdTe Compton camera and its applications to the visualization of radioactive substances, Nucl. Instrum. Methods A. 787 (2015) 207–211.
[6] C.G. Wahl, W.R. Kaye, W. Wang, F. Zhang, J.M. Jaworski, A. King, Y.A. Boucher, Z. He, The Polaris-H imaging spectrometer, Nucl. Instrum. Methods A. 784 (2015) 377–381.
[7] F. Hueso-González, G. Pausch, J. Petzoldt, K.E. Römer, W. Enghardt, Prompt gamma rays detected with a BGO block Compton camera reveal range deviations of therapeutic proton beams, IEEE Trans. Radiat. Plasma Med. Sci. 1 (2017) 76–86.
[8] Y.S. Kim, J.H. Kim, H.S. Lee, H.R. Lee, J.H. Park, J.H. Park, H. Seo, C. Lee, S.H. Park, C.H. Kim, Development of Compton imaging system for nuclear material monitoring at pyroprocessing test-bed facility, J. Nucl. Sci. Technol. 53 (2016) 2040–2048.
[9] Y. Shikaze, Y. Nishizawa, Y. Sanada, T. Torii, J. Jiang, K. Shimazoe, H. Takahashi, M. Yoshino, S. Ito, T. Endo, K. Tsutsumi, S. Kato, H. Sato, Y. Usuki, S. Kurosawa, K. Kamada, A. Yoshikawa, Field test around Fukushima Daiichi nuclear power plant site using improved Ce:Gd3(Al,Ga)5O12 scintillator Compton camera mounted on an unmanned helicopter, J. Nucl. Sci. Technol. 53 (2016) 1907–1918.
[10] J.E. Gormley, W.L. Rogers, N.H. Clinthorne, D.K. Wehe, G.F. Knoll, Experimental comparison of mechanical and electronic gamma-ray collimation, Nucl. Instrum. Methods A. 397 (1997) 440–447.
[11] L.E. Smith, C. Chen, D.K. Wehe, Z. He, Hybrid collimation for industrial gamma-ray imaging: combining spatially coded and Compton aperture data, Nucl. Instrum. Methods A. 462 (2001) 576–587.
[12] W. Lee, D.K. Wehe, Simulation Results of a Dual Aperture Gamma Ray Imager, IEEE Nuclear Science Symposium Conference Record, Puerto Rico, 2005.
[13] W. Lee, D.K. Wehe, Hybrid gamma ray imaging - model and results, Nucl. Instrum. Methods A. 579 (2007) 200–204.
[14] W. Lee, D.K. Wehe, M. Jeong, P. Barton, J. Berry, Dual modality gamma camera using LaCl3(Ce) scintillators, IEEE Trans. Nucl. Sci. 56 (2009) 308–315.
[15] T. Lee, W. Lee, Compact hybrid gamma camera with a coded aperture for investigation of nuclear materials, Nucl. Instrum. Methods A. 767 (2014) 5–13.
[16] L.J. Schultz, M.S. Wallace, M.C. Galassi, A.S. Hoover, M. Mocko, D.M. Palmer, S.R. Tornga, R.M. Kippen, M.V. Hynes, M.J. Toolin, B. Harris, J.E. McElroy, D. Wakeford, R.C. Lanza, B.K.P. Horn, D.K. Wehe, Hybrid coded aperture and Compton imaging using an active mask, Nucl. Instrum. Methods A. 608 (2009) 267–274.
[17] M. Galloway, A. Zoglauer, S.E. Boggs, M. Amman, A combined Compton and coded-aperture telescope for medium-energy gamma-ray astrophysics, Astron. Astrophys. 614 (2018) A93.
[18] S.R. Gottesman, E.E. Fenimore, New family of binary arrays for coded aperture imaging, Appl. Optic. 28 (1989) 4344–4352.
[19] Y.S. Kim, J.H. Kim, H.S. Lee, C.H. Kim, Position-sensitive NaI(Tl) detector module for large-area Compton camera, J. Kor. Phys. Soc. 72 (2018) 26–32.
[20] L.R. Furenlid, J.Y. Hesterman, H.H. Barrett, Fast maximum-likelihood estimation methods for scintillation cameras and other optical sensors, Proc. SPIE-Int. Soc. Opt. Eng. 6707 (2007) 67070N.
[21] H.S. Lee, J.H. Kim, J. Lee, C.H. Kim, Design and performance prediction of large-area hybrid gamma imaging system (LAHGIS) for localization of low-level radioactive material, Nucl. Eng. Technol. (2020), https://doi.org/10.1016/j.net.2020.09.008. In press.
[22] L.A. Shepp, Y. Vardi, Maximum likelihood reconstruction for emission tomography, IEEE Trans. Med. Imag. 1 (2) (1982) 113–122.
[23] E. Munoz, J. Barrio, J. Bernabeu, A. Etxebeste, C. Lacasta, G. Llosa, A. Ros, J. Roser, J.F. Oliver, Study and comparison of different sensitivity models for a two-plane Compton camera, Phys. Med. Biol. 63 (2018) 135004.